Supplementary Information (SI) for Journal of Materials Chemistry C.

Supporting Information

Defect healing and improved hole transport in CuSCN by copper(I) halides

Patipan Sukpoonprom,[a] Pinit Kidkhunthod,[b] Chitsanucha Chattakoonpaisarn,[a]
Somlak Ittisanronnachai,[c] Taweesak Sudyoadsuk,[c] Vinich Promarak,[a]
and Pichaya Pattanasattayavong[a,*]

[a] Department of Materials Science and Engineering, School of Molecular Science and Engineering, Vidyasirimedhi Institute of Science and Technology (VISTEC), Rayong 21210, Thailand

[b] Synchrotron Light Research Institute (Public Organization), 111 University Avenue, Muang, Nakhon Ratchasima 30000, Thailand

[c] Frontier Research Center (FRC), Vidyasirimedhi Institute of Science and Technology (VISTEC), Rayong 21210, Thailand

* Correspondence: pichaya.p@vistec.ac.th

Experimental section

Preparation of CuSCN solutions. Copper(I) thiocyanate (CuSCN) and copper(I) halides (CuX, X = Cl, Br, or I) were purchased from Sigma-Aldrich and used as-received without purification. CuSCN was dissolved in diethyl sulfide (DES, 98%, TCI) at a concentration of 10 and 11 mg mL^{-1} for reference and doping conditions, respectively. The solution was stirred at room temperature for 4 h and filtered through a 0.22-μm PTFE syringe filter. For the doping process, CuX dopants were also dissolved separately in DES. Then, 500 μL of 11 mg mL^{-1} CuSCN solution was added with 50 μL of CuX solution to obtain a final solution having the same CuSCN concentration of 10 mg mL^{-1} as the reference condition. The concentrations of the CuX solutions were varied to study the effect of doping concentration as described in **Table S1**. The doping concentration (% doping) was calculated from the percentage of the mole ratio between CuX and CuSCN, i.e., $(\mathrm{mol}_{\mathrm{CuX}}/\mathrm{mol}_{\mathrm{CuSCN}})\times100$. The mixed solutions were stirred overnight before use.

Thin-film transistor (TFT) fabrication and measurements. Borosilicate glass was used as the substrate. All substrates were sequentially cleaned a 1%v/v detergent solution (Liquinox, Alconox Inc.), deionized water, acetone, and isopropanol in an ultrasonic bath for 10 min each, and then dried with N_2 gun. Bottom-gate top-contact (BG-TC) TFTs were fabricated on the cleaned substrates using thermally evaporating 40 nm-thick Al as the gate (G) electrode through a shadow mask. The Al gate layer was treated with UV-ozone for 10 minutes to improve wettability and transferred to a N_2-filled glove box. Poly(vinylidene fluoride-trifluoroethylene-chlorofluoroethylene) or P(VDF-TrFE-CFE) (63/30/7 mol%, PolyK Technologies), dissolved in 2-butanone (>99%, TCI) at 40 mg mL^{-1}, was deposited on Al gate by spin-casting at 1000 rpm at room temperature for 40 s. As-spun films were annealed at 80 °C for 3 h to obtain the bottom dielectric layer with a geometric capacitance of 96 nF cm^{-2}. Next, pristine or CuX-doped CuSCN solution was spin-cast onto the dielectric layer at 2000 rpm for 60 s and annealed at 100 °C for 20 min. Finally, 25-nm Au was deposited by thermal evaporation through a shadow mask to construct the source/drain electrodes. Device dimensions: channel width (W) of 1000 μm and channel length (L) of 30, 40, 50, 80, and 100 μm. Transistors were characterized using a Keysight B2912A 2-channel source-measure unit (SMU) under dry N_2 atmosphere in a glove box. TFT parameters, i.e., linear and saturation mobility (μ_{lin} and μ_{sat}), threshold voltage (V_{th}), were determined based on the standard gradual channel approximation.[1] Transfer characteristics of devices with L = 30 μm were used for the analyses. Subthreshold swing (S_{th}) and relative interfacial trap density (ΔN_{tr}) were calculated by:[2]

$$S_{\text{th}} = \frac{\partial V_{\text{G}}}{\partial(\log I_{\text{D}})} \tag{S1}$$

where V_G and I_D are the gate voltage and drain current, respectively; and

$$\Delta N_{\text{tr}} = \frac{C_i\,\Delta V_{\text{th}}}{q} \tag{S2}$$

where C_i is the geometric capacitance of the dielectric, q the elementary charge.

Contact resistance (R_c) analysis was performed using the gated transfer length method.[3] R_c was evaluated from the output characteristics in the linear regime from devices with various channel lengths. The total resistance (R_t) can be expressed as:

$$R_{\text{t}}W = \frac{L}{\mu_{\text{lin}}C_{\text{i}}(V_{\text{G}}-V_{\text{th}})} - R_{\text{c}}W \tag{S3}$$

Note that R_t and R_c are expressed as channel width-normalized quantities, R_tW and R_cW. The contact resistance R_cW can be obtained from the y-intercept of the plot between R_tW and L.

Ultraviolet-visible-near-infrared spectroscopy (UV-vis-NIR). All samples were deposited on JGS3 fused silica substrates (Xin Yan Technology Limited) to avoid UV absorption of the substates. Transmission spectra were recorded using a Perkin Elmer LAMBDA 1050 spectrophotometer in a range of 200-800 nm. The absorption spectra were calculated using Beer-Lambert law. The optical band gaps were calculated using Tauc plots.

Photoelectron yield Spectroscopy (PYS) and Kelvin probe (KP) measurement. All samples were spin-coated onto ITO substrates using the same procedure for device fabrication. The valence band maxima (VBM), i.e., obtained from the ionization potentials (IPs), were measured using a RIKEN AC-2 photoelectron spectrometer in air. The UV excitation was generated by a deuterium arc lamp and monochromated by a grating. For semiconductors, IPs were determined from the threshold energies of the yield$^{1/3}$ spectra. The Kelvin probe measurement was performed with a KP Technology KP020 system to determine the work function (WF) of the films. Contact potential differences (CPDs) of the samples were measured with respect to an Au reference of a known WF value (4.74 eV, measured by PYS). All measurements were done under ambient conditions.

Atomic force microscopy (AFM). Films were prepared in the same method as described for TFT fabrication on the P(VDF-TrFE-CFE) dielectric layer. Surface topography was probed by a Park Systems NX10 in a non-contact mode with an Olympus OMCL-AC160TS cantilever. Surface height histograms and root-mean-square roughness were analyzed from images of an area of 5 μm × 5 μm and using Gwyddion software.[4]

X-ray diffraction (XRD). To acquire good signals, drop-cast samples were used for the measurements in the powder mode. Samples were prepared by drop-casting solutions on borosilicate glass and dried for 10 min. Substrates were pre-heated to 100 °C and maintained at that temperature during casting. XRD data was acquired using a Bruker D8 Advance diffractometer with a Cu K_α X-ray source (λ = 1.5406 Å). The diffraction patterns were scanned for 2θ range between 10° to 60° with an increment of 0.05°.

X-ray photoelectron spectroscopy (XPS). Chemical bonding states of the films were characterized with a JEOL JPS9010MC photoelectron spectrometer using a monochromatic Al K_α source (1486.6 eV) operated at 12 kV and 25 mA under a base pressure of 10^{-7} Pa with a low-energy electron flood gun to reduce charging. Data were recorded at a pass energy of 50 eV for survey scans and 10 eV for high-resolution core-level scans. The spectra were averaged from 60 scans. Before loading the samples, they were kept in a vacuum antechamber overnight to minimize the water and oxygen molecules on the film surface. All obtained spectra and elemental quantification were analyzed by SpecSurf software and referenced to adventitious carbon C 1s at 284.8 eV.

X-ray absorption spectroscopy (XAS). Oxidation state and local atomic environment around Cu were characterized by XAS at beamline BL5.2 SUT-NANOTEC-SLRI, Synchrotron Light Research Institute (SLRI), Nakhon Ratchasima, Thailand (electron energy 1.2 GeV, bending magnet, beam current 80-150 mA). CuSCN powder purchased from Sigma-Aldrich was used as a standard sample (denoted as 'CuSCN standard') whereas CuSCN processed from DES solution with the same procedure but without dopants was used as a control sample (denoted as 'Undoped CuSCN'). Samples were prepared by drop-casting, using the same preparation method for XRD. Before the measurements, the samples were carefully packed in Kapton-covered holders. Both the X-ray absorption near edge structure (XANES) and the extended X-ray absorption fine structure (EXAFS) at Cu K-edge were acquired in transmission mode under ambient conditions. The spectra were averaged from three scans and processed by the standard procedure using ATHENA software (Demeter package).[5]

References

(1) Thomas, S. R.; Pattanasattayavong, P.; Anthopoulos, T. D. Solution-Processable Metal Oxide Semiconductors for Thin-Film Transistor Applications. *Chem. Soc. Rev.* **2013**, *42* (16), 6910–6923. https://doi.org/10.1039/c3cs35402d.

(2) Sze, S. M.; Ng, K. K. *Physics of Semiconductor Devices: Third Edition*; 2006. https://doi.org/10.1002/9780470068328.

(3) Waldrip, M.; Jurchescu, O. D.; Gundlach, D. J.; Bittle, E. G. Contact Resistance in Organic Field-Effect Transistors: Conquering the Barrier. *Adv. Funct. Mater.* **2020**, *30* (20), 1904576. https://doi.org/10.1002/adfm.201904576.

(4) Nečas, D.; Klapetek, P. Gwyddion: An Open-Source Software for SPM Data Analysis. *Central European Journal of Physics*. February 2012, 181–188. https://doi.org/10.2478/s11534-011-0096-2.

(5) Ravel, B.; Newville, M. ATHENA, ARTEMIS, HEPHAESTUS: Data Analysis for X-Ray Absorption Spectroscopy Using IFEFFIT. In *Journal of Synchrotron Radiation*; 2005; Vol. 12, 537–541. https://doi.org/10.1107/S0909049505012719.

Table S1. Solution concentrations for each doping condition.

Dopant	% Doping*	Concentration (mg/mL)	Solution volume (μL)	Mass of CuSCN (mg)	Mole of CuSCN (mol)	Mass of CuX (mg)	Mole of CuX (mol)	Initial halide mol.%	Found halide at.% from XPS
None (stock CuSCN solution for doping)	-	11	500	5.5	4.5×10^{-5}	-	-	-	-
CuCl	1%	0.90	50	5.5	4.5×10^{-5}	0.045	4.5×10^{-7}	1.0	-
	3%	2.7	50	5.5	4.5×10^{-5}	0.13	1.4×10^{-6}	2.9	1.01
	5%	4.5	50	5.5	4.5×10^{-5}	0.22	2.3×10^{-6}	4.8	1.35
	7%	6.3	50	5.5	4.5×10^{-5}	0.31	3.2×10^{-6}	6.5	1.50
CuBr	1%	1.3	50	5.5	4.5×10^{-5}	0.065	4.5×10^{-7}	1.0	-
	3%	3.9	50	5.5	4.5×10^{-5}	0.19	1.4×10^{-6}	2.9	0.80
	5%	6.5	50	5.5	4.5×10^{-5}	0.32	2.3×10^{-6}	4.8	2.01
	7%	9.1	50	5.5	4.5×10^{-5}	0.45	3.2×10^{-6}	6.5	2.81
CuI	1%	1.7	50	5.5	4.5×10^{-5}	0.086	4.5×10^{-7}	1.0	0.50
	3%	5.2	50	5.5	4.5×10^{-5}	0.26	1.4×10^{-6}	2.9	1.22
	5%	8.6	50	5.5	4.5×10^{-5}	0.43	2.3×10^{-6}	4.8	1.84
	7%	12	50	5.5	4.5×10^{-5}	0.60	3.2×10^{-6}	6.5	2.54

* % Doping = $[(\mathrm{mol}_{\mathrm{CuX}}/\mathrm{mol}_{\mathrm{CuSCN}})\times100]$

Table S2. Summary of TFT parameters averaged from 10 different devices for each condition.

Dopant	% Doping	μ_{lin} (10^{-2} cm^2 V^{-1} s^{-1})			μ_{sat} (10^{-2} cm^2 V^{-1} s^{-1})			V_{th} (V)			S_{th} (V dec^{-1})			D_{tr} (10^{13} cm^{-2} eV^{-1})			I_{on} (μA)		I_{off} (nA)		I_{on}/I_{off} ratio (×10^4)	
		Max	Avg	SD	Max	Avg	SD	|Min|	Avg	SD	Min	Avg	SD	Min	Avg	SD	Avg	SD	Avg	SD	Avg	SD
Undoped	-	0.99	0.97	0.02	1.20	1.01	0.13	-6.83	-6.45	0.12	4.30	5.14	0.44	4.29	5.15	0.45	10.0	1.1	1.50	0.37	0.70	0.14
CuCl	1	3.18	2.89	0.16	3.71	3.33	0.21	-5.27	-4.74	0.52	2.98	3.13	0.16	2.96	3.11	0.17	34.3	3.0	1.68	0.34	2.10	0.34
	3	4.22	3.92	0.14	4.25	4.08	0.14	-4.03	-3.53	0.35	2.75	3.29	0.27	2.72	3.28	0.27	45.3	2.9	3.92	0.91	1.21	0.26
	5	2.72	2.62	0.09	2.95	2.79	0.09	-4.20	-3.59	0.40	3.11	3.66	0.28	3.09	3.65	0.28	30.5	1.5	3.16	0.82	1.06	0.40
	7	1.60	1.50	0.12	1.65	1.56	0.10	-4.30	-4.09	0.16	3.30	3.71	0.26	3.28	3.70	0.27	16.3	1.1	1.92	0.47	0.94	0.30
CuBr	1	3.06	2.88	0.13	3.26	3.11	0.14	-6.14	-5.55	0.32	2.97	3.44	0.28	2.95	3.43	0.29	29.5	1.5	1.63	0.47	1.96	0.61
	3	4.23	3.96	0.21	4.81	4.25	0.33	-5.04	-4.24	0.54	2.67	3.16	0.27	2.64	3.14	0.27	44.4	2.7	2.25	0.92	2.02	0.64
	5	4.91	4.62	0.17	5.38	5.07	0.16	-4.54	-3.53	0.50	1.88	2.50	0.33	1.84	2.47	0.34	52.3	3.1	1.86	0.35	2.90	0.54
	7	4.26	4.00	0.20	5.09	4.34	0.39	-4.94	-3.78	0.56	2.99	3.66	0.45	2.97	3.65	0.45	47.1	3.5	3.21	1.07	1.66	0.70
CuI	1	2.64	2.49	0.12	2.77	2.50	0.16	-6.00	-5.74	0.31	2.98	3.43	0.30	2.69	3.42	0.31	22.9	1.3	2.57	1.61	1.16	0.51
	3	2.49	2.20	0.16	2.70	2.29	0.21	-5.70	-5.13	0.32	2.80	3.20	0.24	2.78	3.18	0.25	22.4	2.3	1.51	0.39	1.58	0.45
	5	1.81	1.61	0.13	1.93	1.64	0.16	-6.00	-5.59	0.23	2.93	3.37	0.49	2.91	3.36	0.49	15.6	1.7	1.70	0.95	1.17	0.54
	7	1.26	1.15	0.10	1.41	1.20	0.13	-5.66	-5.31	0.29	3.18	3.59	0.31	3.16	3.58	0.32	11.5	1.4	1.52	0.38	0.81	0.26

Table S3. Comparison of ΔV_{th}, ΔN_{tr}, and γ parameters of TFT devices from the optimal condition of each dopant.

Sample	ΔV_{th} (V)	ΔN_{tr} (10^{12} cm^{-2})	γ
Undoped CuSCN	N/A	N/A	0.63±0.06
3% CuCl	2.92	1.75	0.21±0.02
5% CuBr	2.92	1.75	0.22±0.05
1% CuI	0.71	0.43	0.39±0.05

Table S4. Electronic energy levels.

Sample	VBM (eV)	Fermi level (eV)	CBM (eV)	Energy gap (eV)
CuSCN	-5.67	-5.21	-1.86	3.81
3% CuCl	-5.61	-5.32	-1.83	3.78
5% CuBr	-5.69	-5.30	-1.90	3.79
1% CuI	-5.63	-5.42	-1.82	3.81

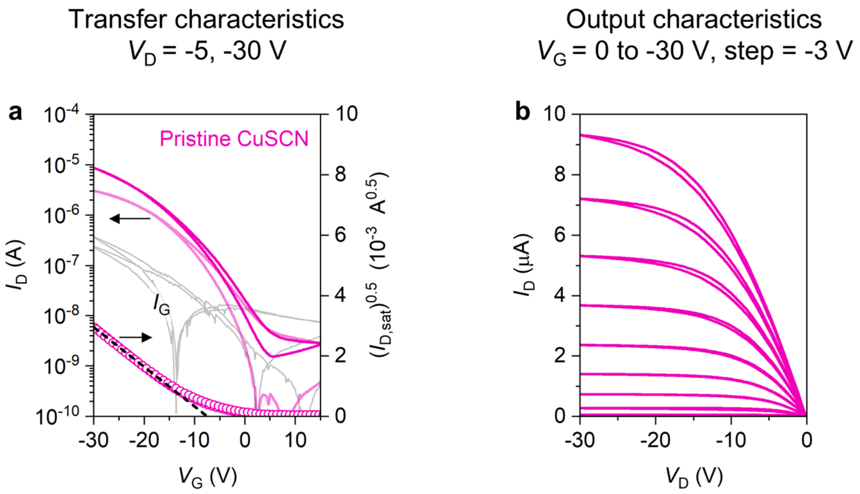

Transfer characteristics
V_D = -5, -30 V

Output characteristics
V_G = 0 to -30 V, step = -3 V

Figure S1. (a-b) Transfer and output characteristics of a representative TFT based on undoped CuSCN.

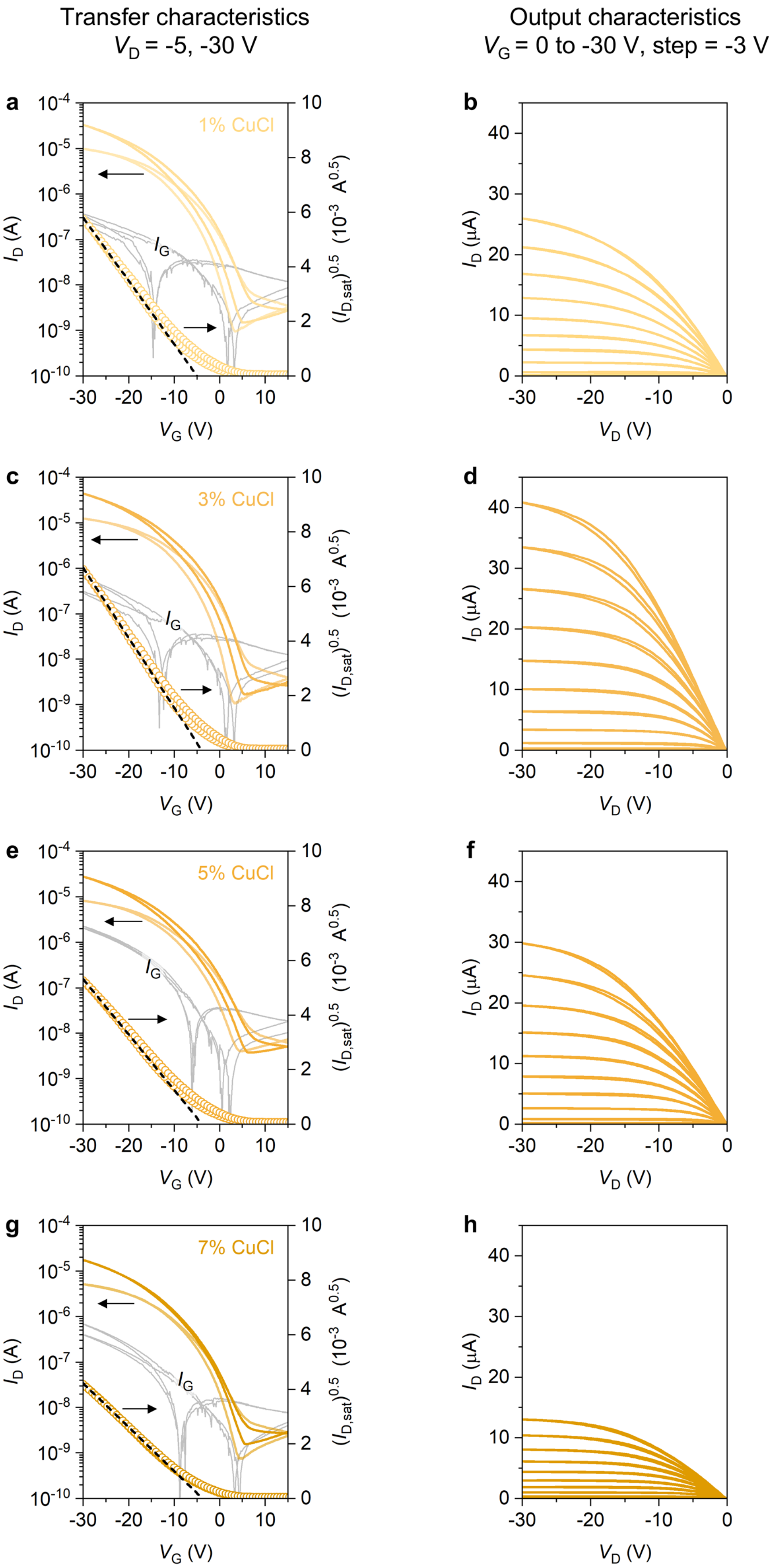

Figure S2. Transfer and output characteristics of representative TFTs based on CuCl-doped CuSCN at: (a-b) 1%, (c-d) 3%, (e-f) 5%, and (g-h) 7% doping.

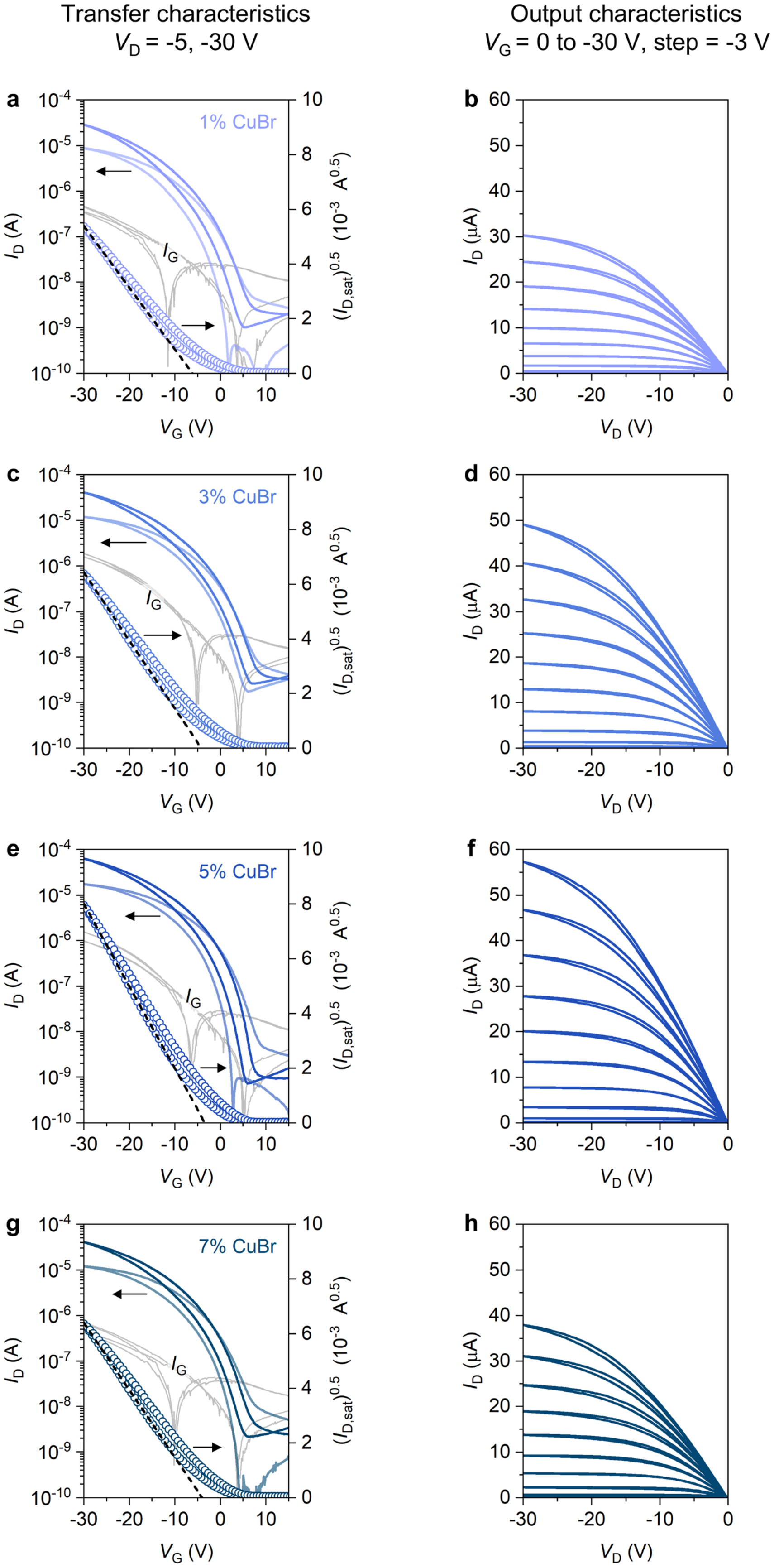

Figure S3. Transfer and output characteristics of representative TFTs based on CuBr-doped CuSCN at: (a-b) 1%, (c-d) 3%, (e-f) 5%, and (g-h) 7% doping.

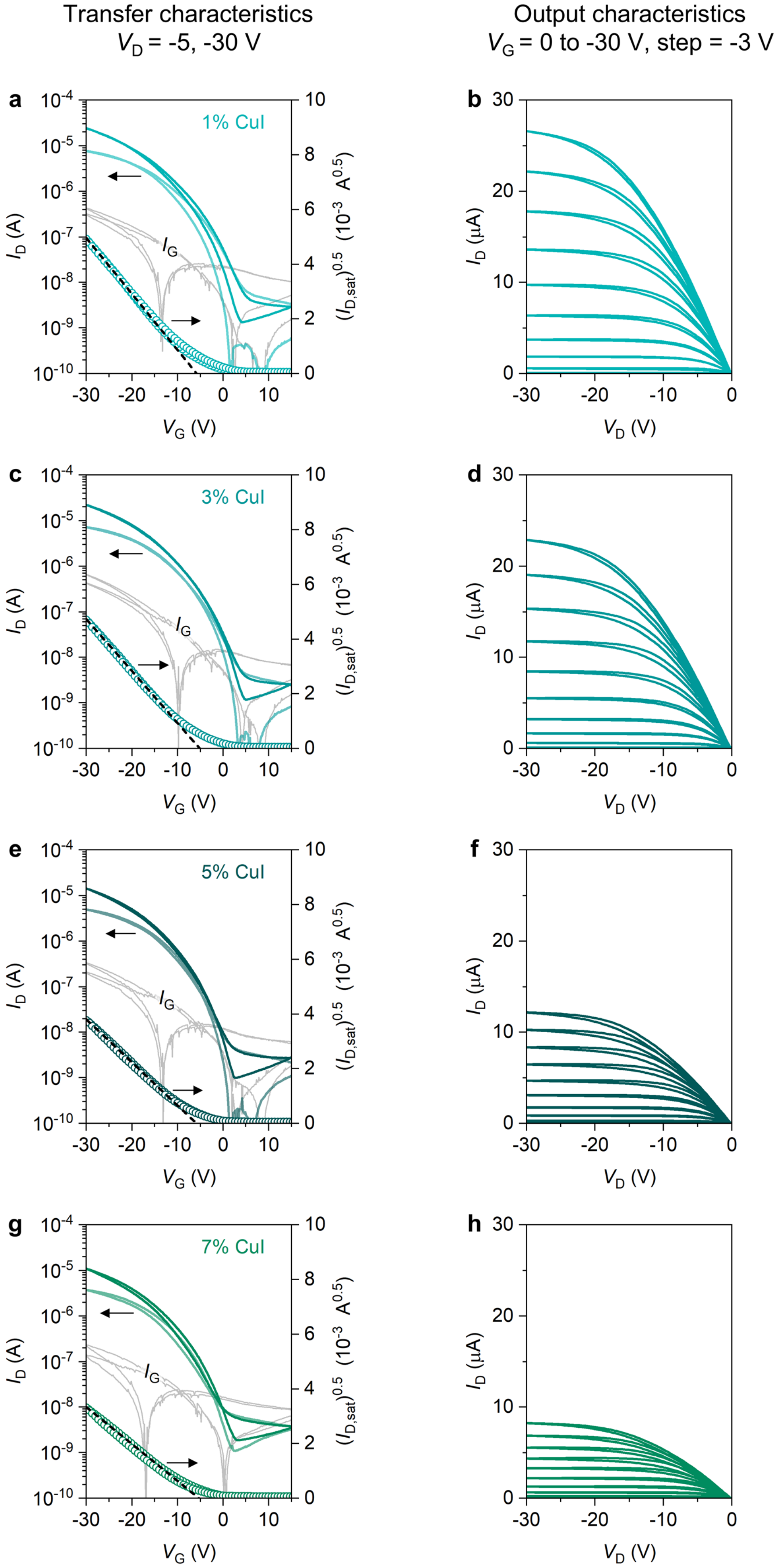

Figure S4. Transfer and output characteristics of representative TFTs based on CuI-doped CuSCN at: (a-b) 1%, (c-d) 3%, (e-f) 5%, and (g-h) 7% doping.

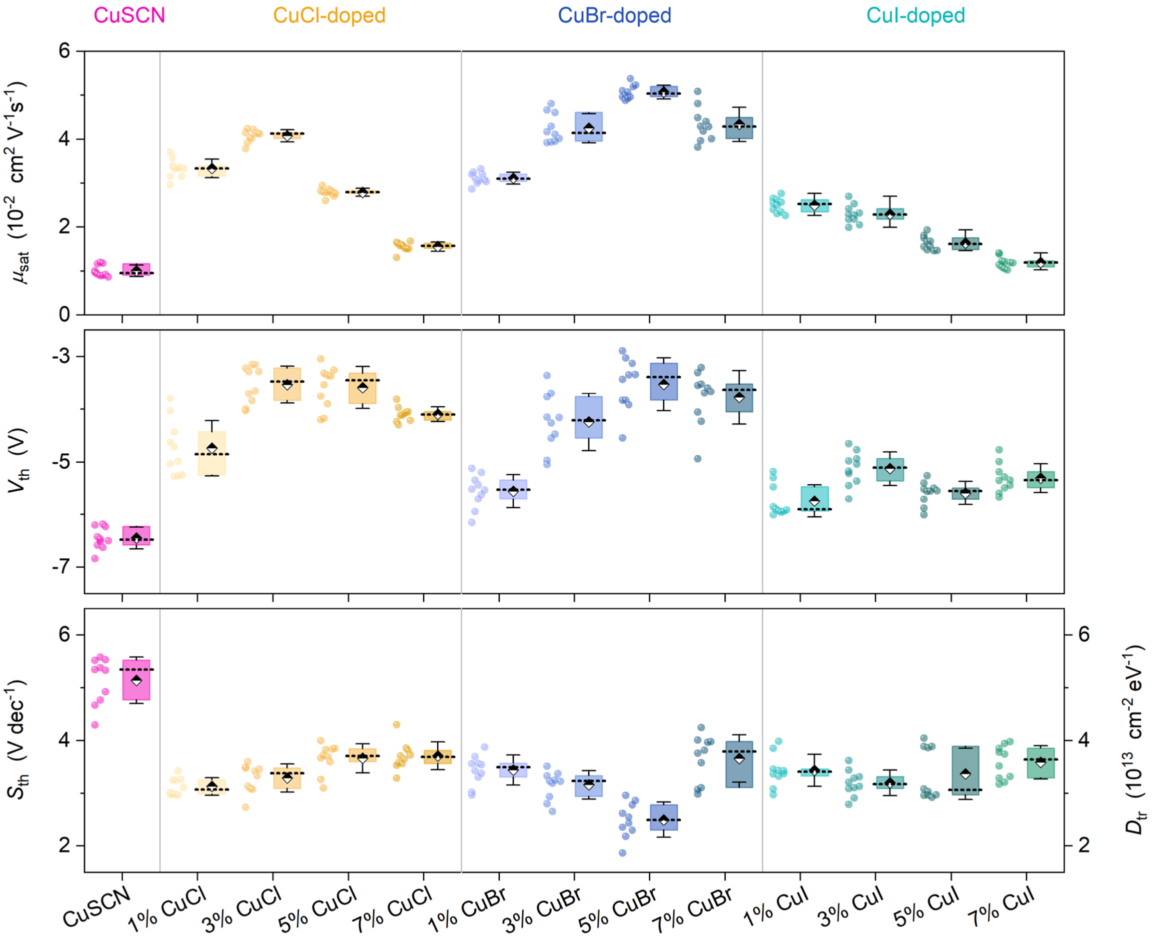

Note: $D_{tr} = \left(1.014 \times 10^{13}\right) S_{th} - \left(6 \times 10^{11}\right)$

Figure S5. Statistics of TFT device parameters. For box plots, the box indicates the 25th and 75th percentiles, dash line the median (50th percentile), half-filled circle the arithmetic mean, and whiskers the standard deviation. Individual data points are shown on the left of the corresponding boxes. D_{tr} is proportional to S_{th} according to Eq. (S2).

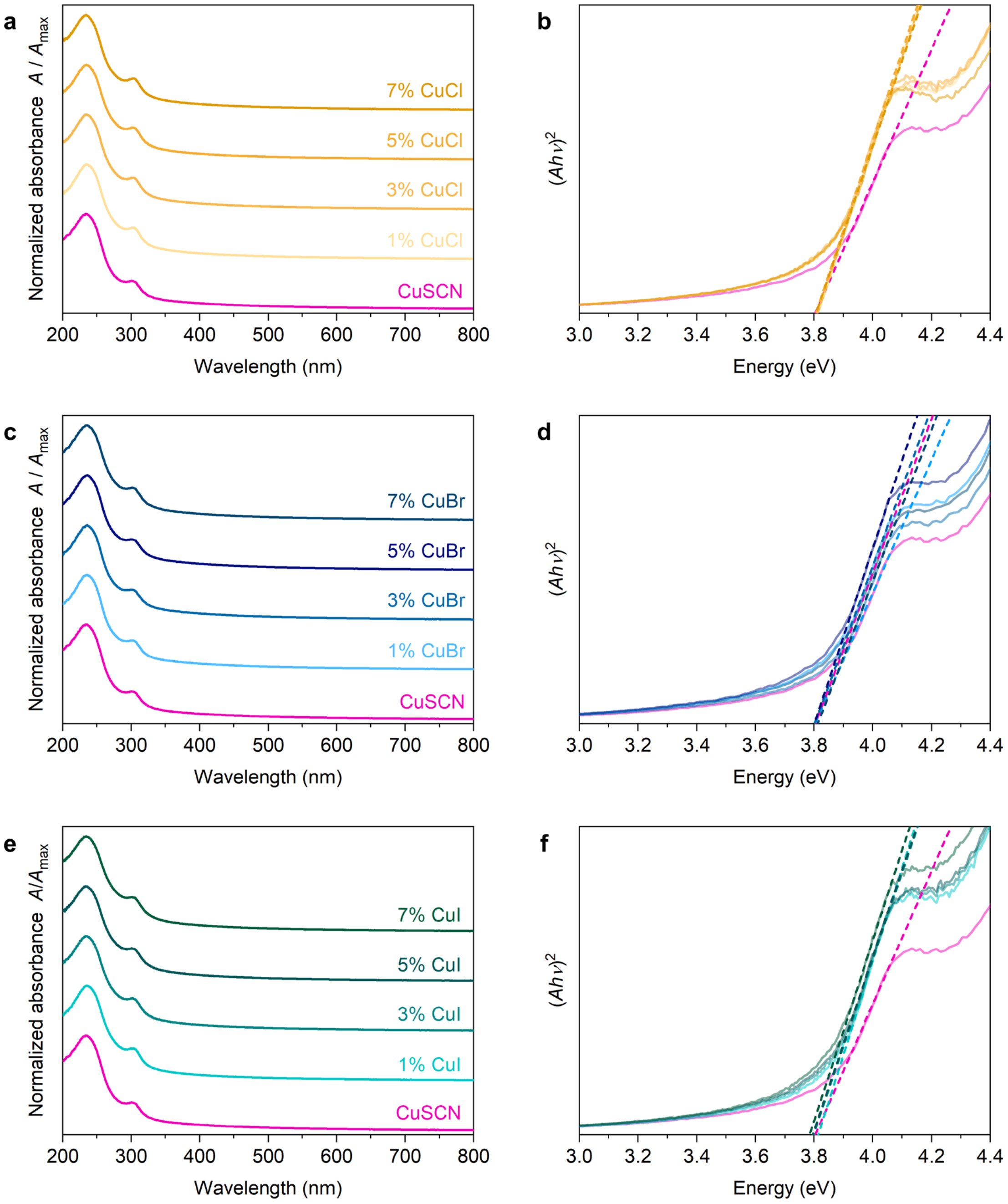

Figure S6. Normalized optical absorbance spectra and Tauc plots of CuSCN films doped with: (a-b) CuCl, (c-d) CuBr, and (e-f) CuI. Data of undoped CuSCN (magenta) is also shown in all plots for reference.

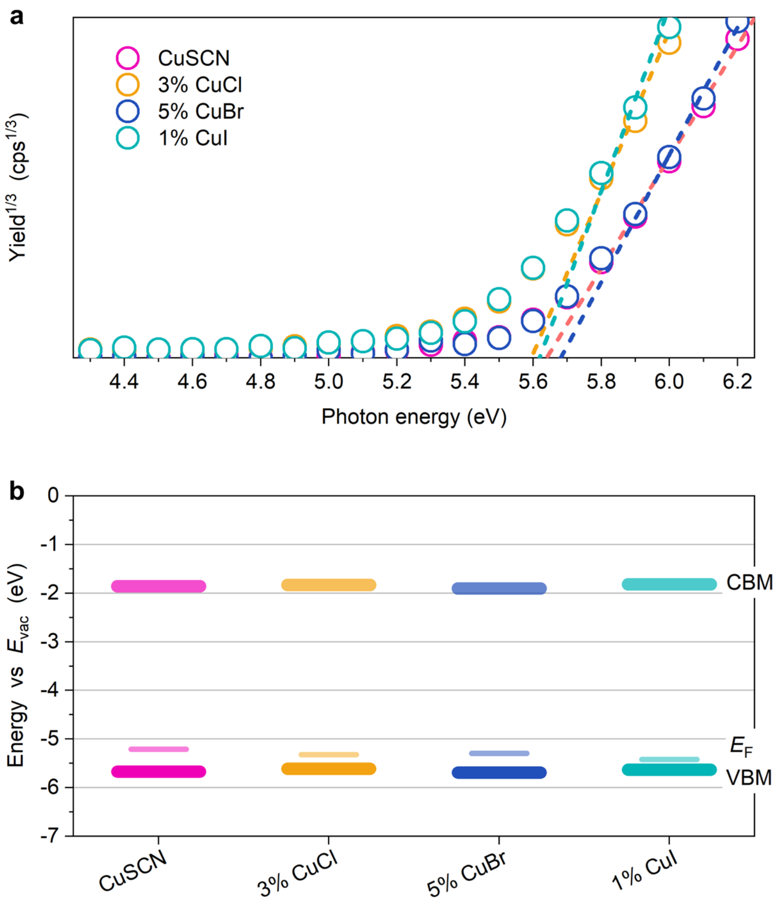

Figure S7. (a) Photoelectron yield spectra. (b) Simplified electronic energy band diagram.

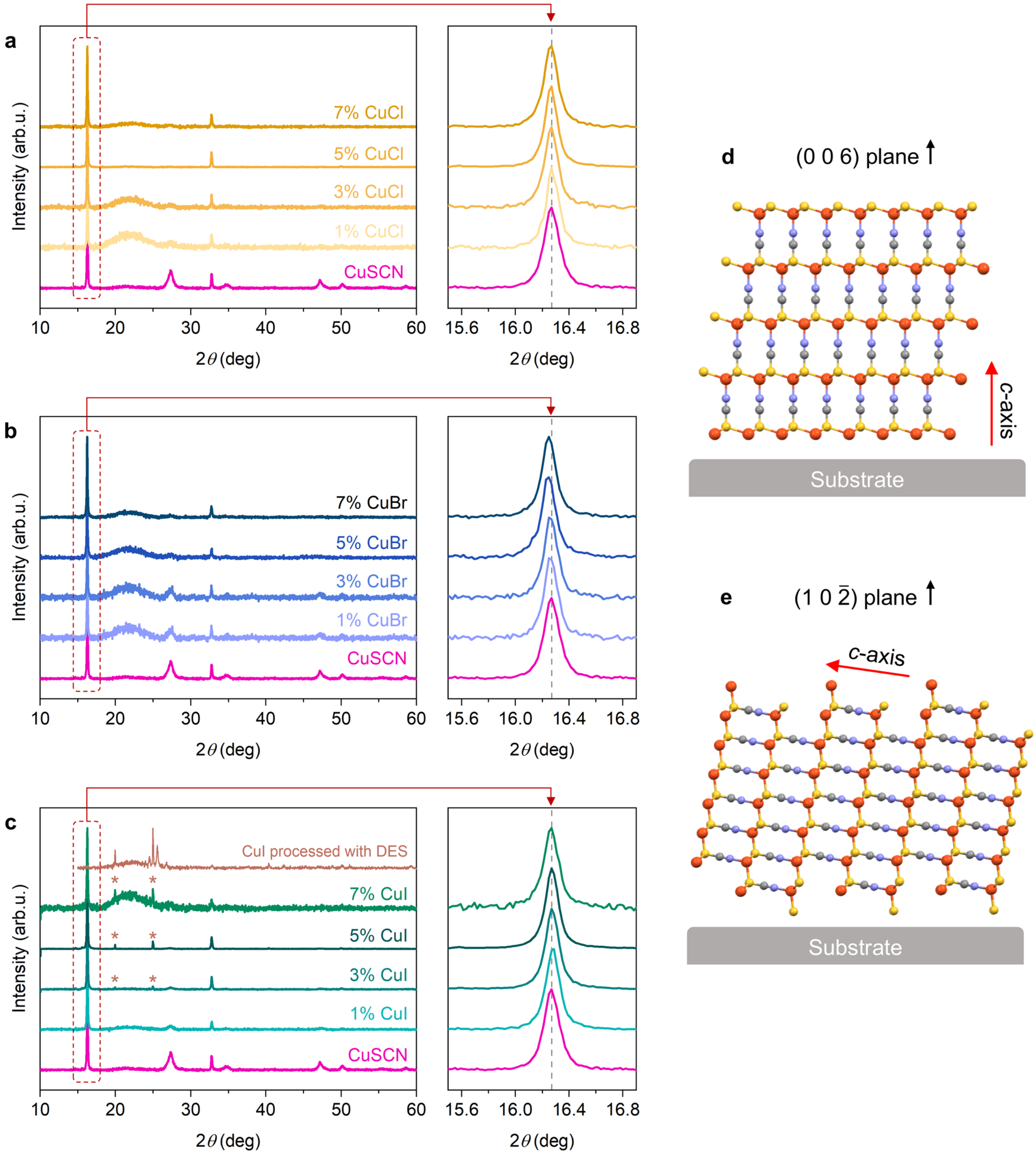

Figure S8. X-ray diffraction patterns of CuSCN samples doped with: (a) CuCl, (b) CuBr, and (c) CuI. Data of undoped CuSCN (magenta) is also shown in all plots for reference. Data of pure CuI also processed with DES is shown in (c) to identify the impurity phase. The panels on the right show the close-up of the (0 0 6) diffraction peaks around 16.3 deg. (d-e) Schematics depicting the '*vertical*' orientation from (0 0 6) diffraction and '*horizontal*' orientation from (1 0 $\bar{2}$) diffraction, respectively.

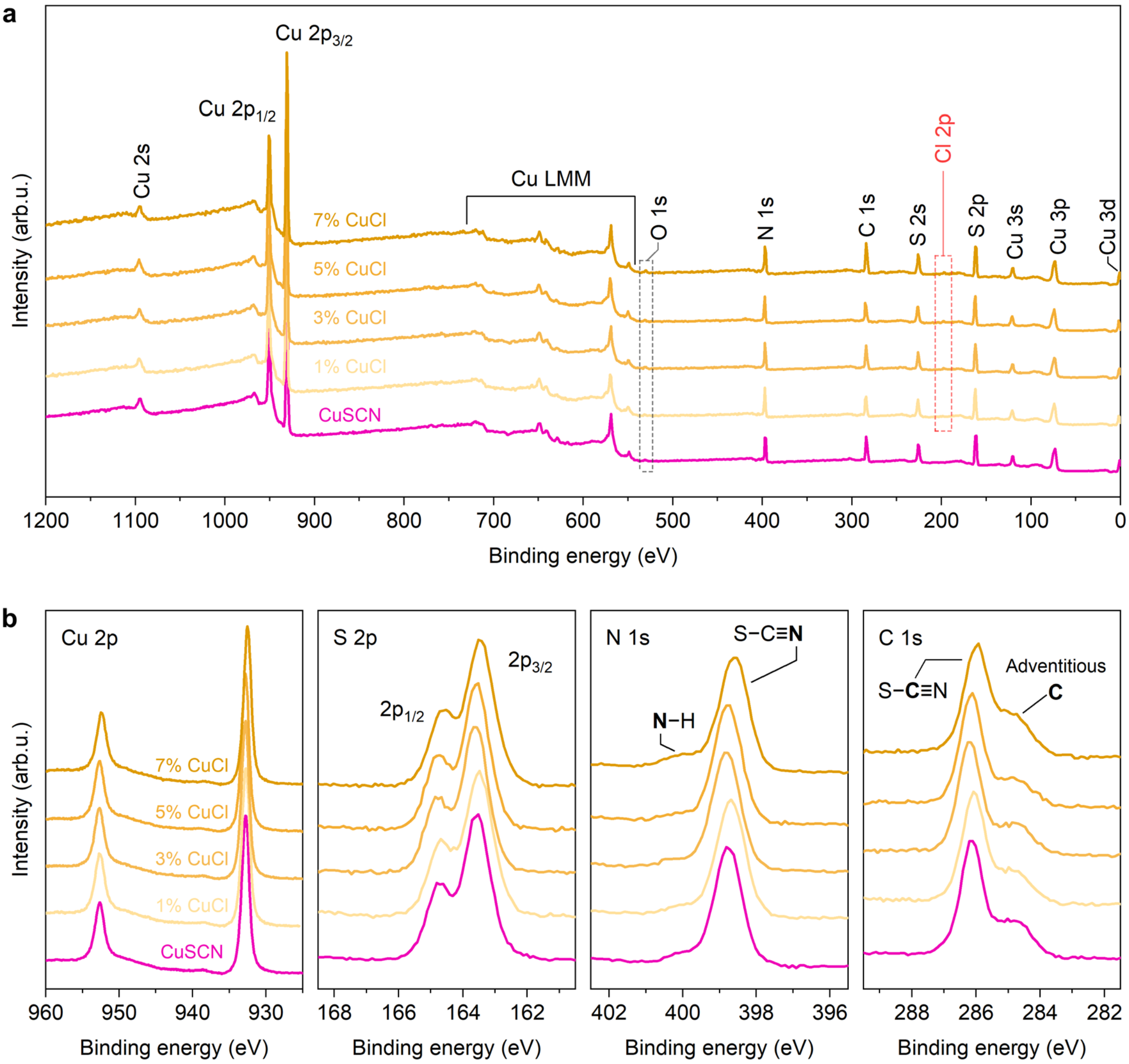

Figure S9. XPS results of CuCl-doped samples: (a) survey scans; and (b) high-resolution core-level scans of Cu 2p, S 2p, N 1s, and C 1s. Data of CuSCN are shown as magenta lines for reference.

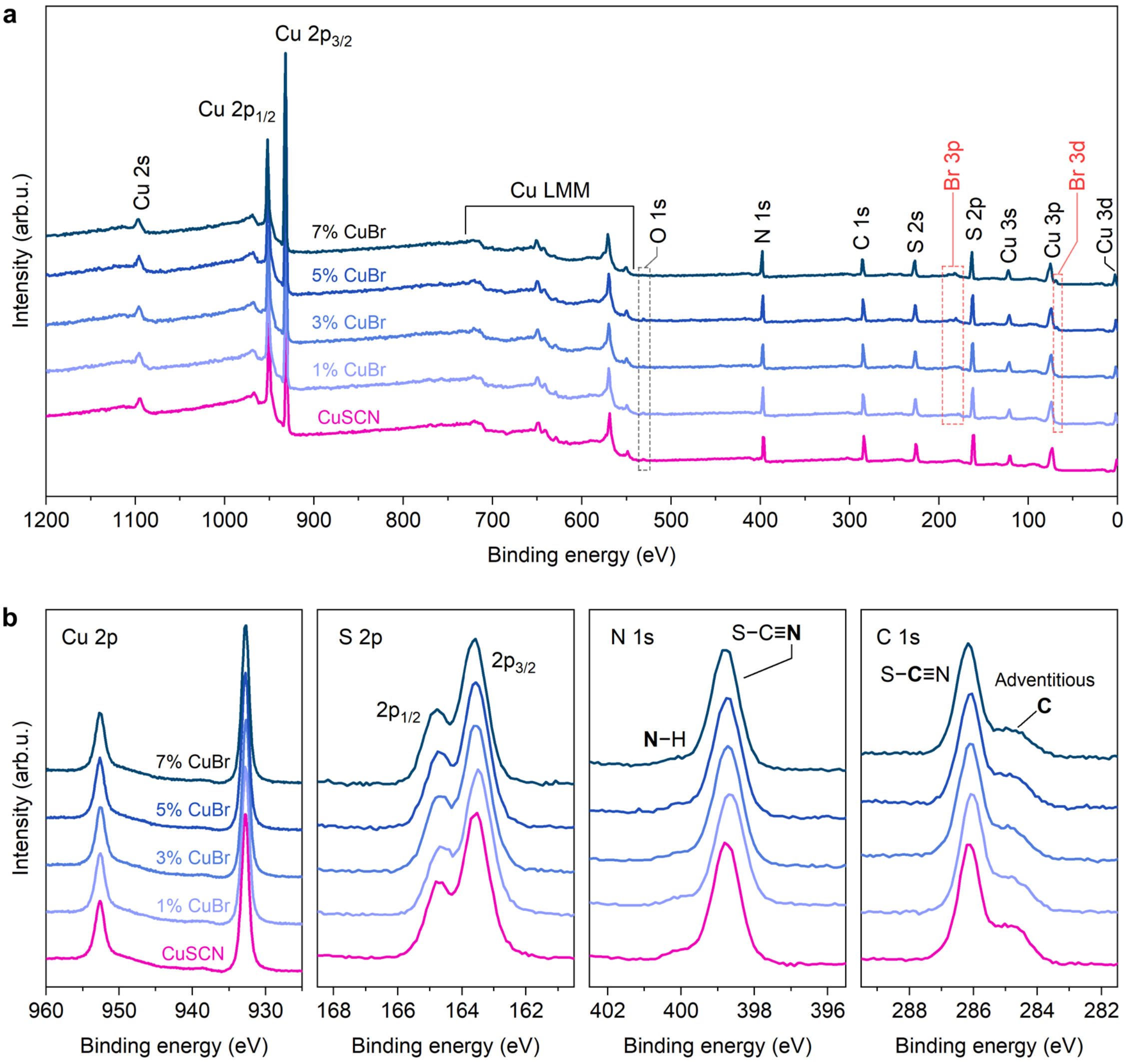

Figure S10. XPS results of CuBr-doped samples: (a) survey scans; and (b) high-resolution core-level scans of Cu 2p, S 2p, N 1s, and C 1s. Data of CuSCN are shown as magenta lines for reference.

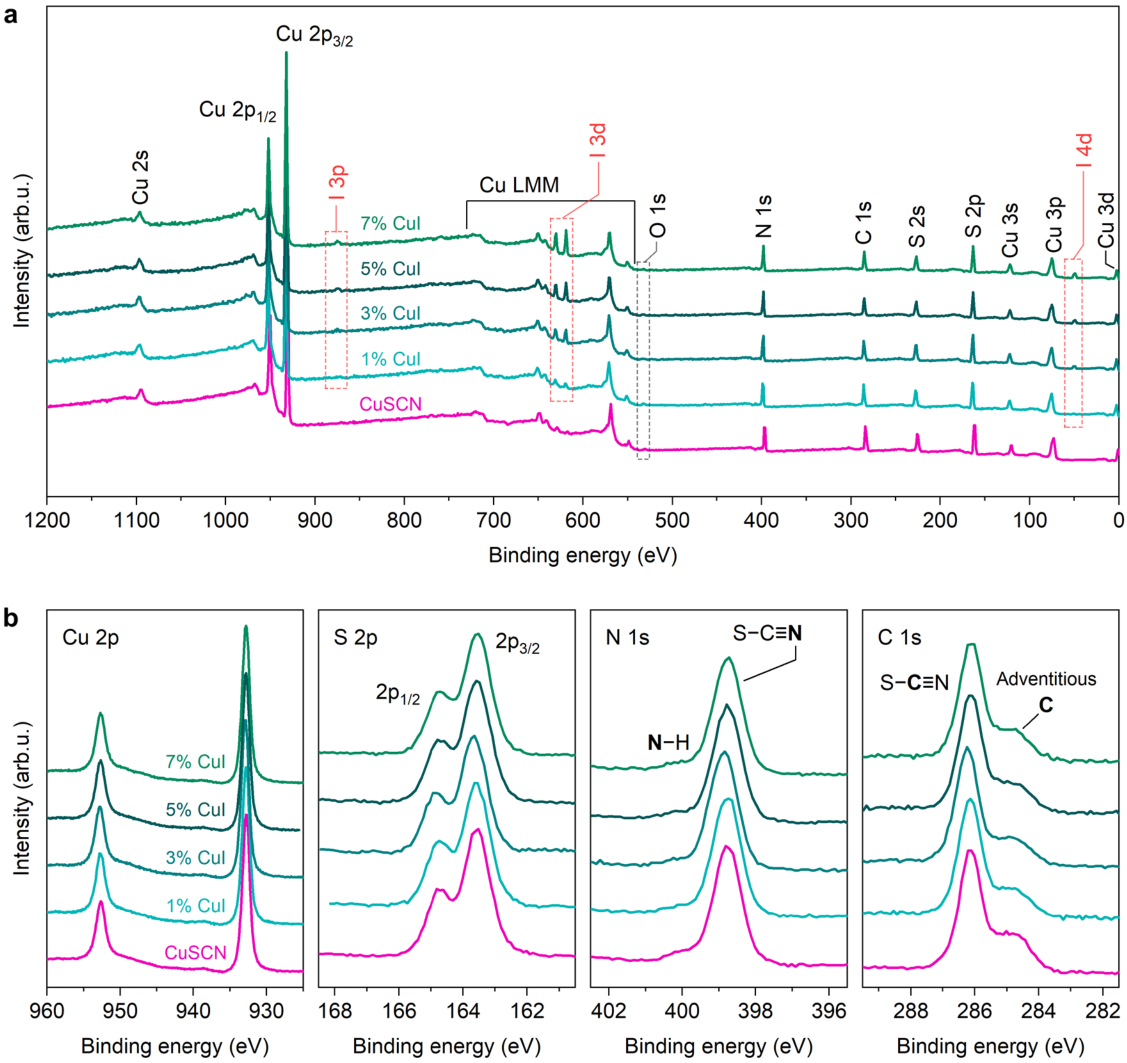

Figure S11. XPS results of CuI-doped samples: (a) survey scans; and (b) high-resolution core-level scans of Cu 2p, S 2p, N 1s, and C 1s. Data of CuSCN are shown as magenta lines for reference.

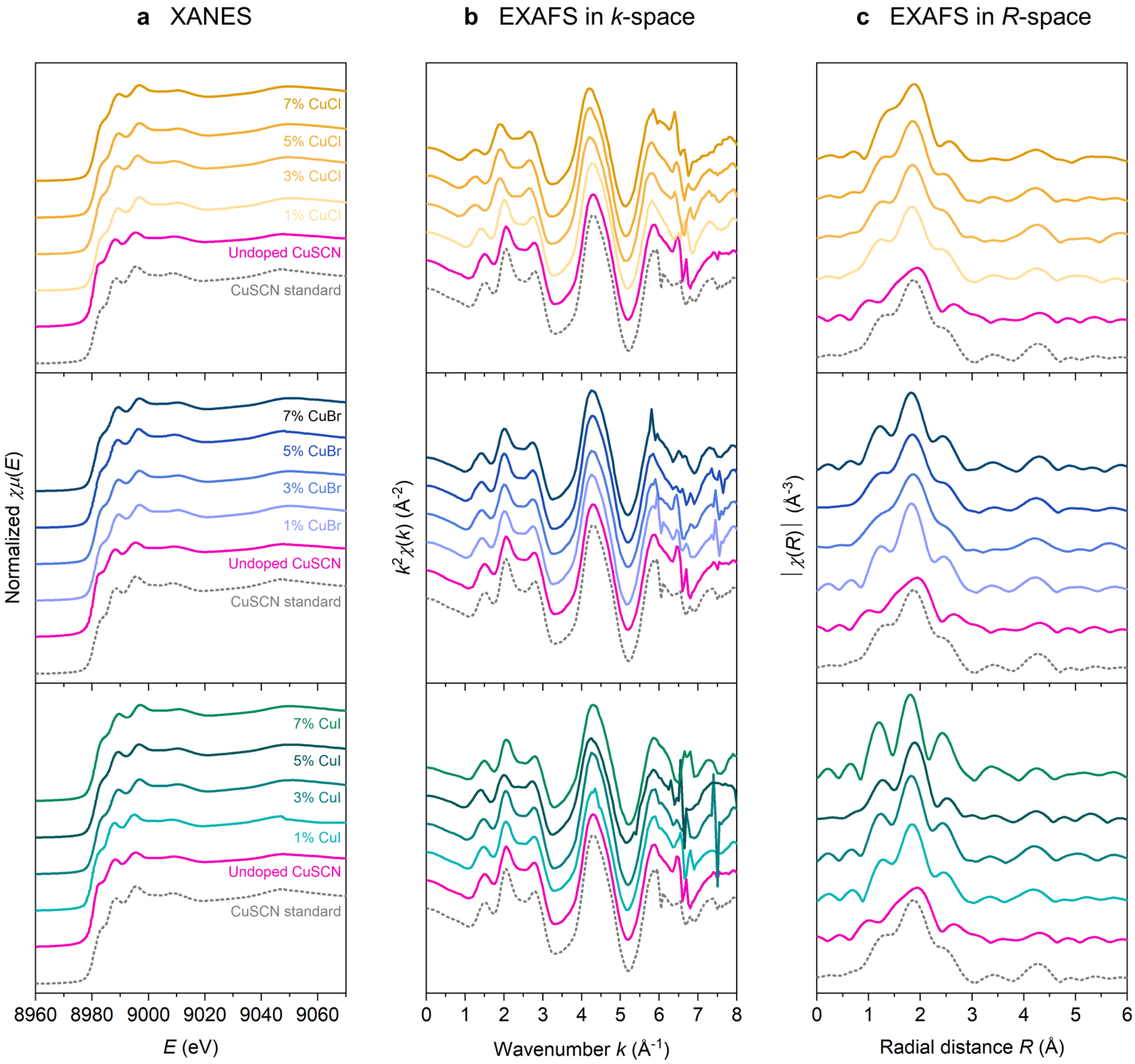

Figure S12. Synchrotron-based XAS results at Cu K-edge: (a) XANES, (b) EXAFS in *k*-space, and (c) EXAFS in *R*-space. In all plots, the dotted lines are data of CuSCN standard (without any solution processing) and the magenta lines the undoped CuSCN sample (solution-processed with DES in the same fashion as the doped samples).